Journal of Applied Physics

Magnetism and magnetocrystalline anisotropy in single-layer $PtSe_2$: Interplay between strain and vacancy

Cite as: J. Appl. Phys. **120**, 013904 (2016); https://doi.org/10.1063/1.4955468
Submitted: 21 March 2016 . Accepted: 25 June 2016 . Published Online: 07 July 2016

Wei Zhang, Hai Tao Guo, Jing Jiang, Qiu Chen Tao, Xiao Jiao Song, Hao Li, and Jie Huang

View Online Export Citation CrossMark

ARTICLES YOU MAY BE INTERESTED IN

Strongly bound excitons in monolayer PtS_2 and $PtSe_2$
Applied Physics Letters **112**, 043101 (2018); https://doi.org/10.1063/1.5010881

The mechanism of layer number and strain dependent bandgap of 2D crystal $PtSe_2$
Journal of Applied Physics **122**, 205701 (2017); https://doi.org/10.1063/1.5000419

Electronic, transport, and optical properties of bulk and mono-layer $PdSe_2$
Applied Physics Letters **107**, 153902 (2015); https://doi.org/10.1063/1.4933302

Lock-in Amplifiers up to 600 MHz
Watch

AIP Publishing

© 2016 Author(s).

Magnetism and magnetocrystalline anisotropy in single-layer $PtSe_2$: Interplay between strain and vacancy

Wei Zhang,[1,a)] Hai Tao Guo,[1,2] Jing Jiang,[1,2] Qiu Chen Tao,[1] Xiao Jiao Song,[1] Hao Li,[1] and Jie Huang[3]

[1]*Physicochemical Group of Department of Criminal Science and Technology, Nanjing Forest Police College, Nanjing 210023, China*

[2]*National Judicial Authentication Center of Public Security Bureau of State Forestry Bureau, Nanjing Forest Police College, Nanjing 210023, China*

[3]*Department of Physics and Institute of Theoretical Physics, Nanjing Normal University, Nanjing 210023, China*

(Received 21 March 2016; accepted 25 June 2016; published online 7 July 2016)

The electronic and magnetic properties of the newly synthesized single-layer (1 L) transition-metal dichalcogenide (TMD) $PtSe_2$ are studied by first-principles calculations. We find the strain or selenium vacancy (V_{Se}) alone cannot induce the magnetism. However, an interplay between strain and V_{Se} leads to the magnetism due to the breaking of Pt-Pt metallic bonds. Different from the case of 1 L-MoS_2 with V_S, the defective 1 L-$PtSe_2$ has the spatially extended spin density, which is responsible for the obtained long range ferromagnetic coupling. Moreover, the 1 L-$PtSe_2$ with V_{Se} undergoes a spin reorientation transition from out-of-plane to in-plane magnetization, accompanying a maximum magnetocrystalline anisotropy energy of ~9–10.6 meV/V_{Se}. These results indicate the strain not only can effectively tune the magnetism but also can manipulate the magnetization direction of 1 L-TMDs. *Published by AIP Publishing.* [http://dx.doi.org/10.1063/1.4955468]

I. INTRODUCTION

Trigged by the successful realization of single-layer (1 L) graphite (the well known graphene),[1,2] the two-dimensional (2D) materials have attracted great attentions because of the peculiar physics brought by them and the potential for next generation of nanoscale device applications.[3–5] The lack of band gap of graphene had been deemed as a considerable drawback for its applications such as switching operation in digital logic devices.[6,7] For this reason, the researchers had turned their attention to other kinds of 2D materials called transition metal dichalcogenides (TMDs),[3–5,8] where the 2D layers could be exfoliated from the stacked crystal structure using the same method as for graphene production.[3,8] The TMDs had a common structural formula MX_2, where M were the transition metals (Mo, W, Pt, etc.) and X were the chalcogens (S, Se, Te, etc.). Among these TMDs, the 1 L-MoS_2 had emerged as a semiconducting alternative to graphene due to its large intrinsic direct bandgap of 1.8 eV.[3,8–15] However, the electron mobility of 1 L-MoS_2 was only up to ten $cm^2/V/s$ at room temperature.[3] A carrier mobility of 200 $cm^2/V/s$ had been reported in the 1 L-MoS_2 based field effect transistors.[8] But recent experiments had shown that the enhanced carrier mobility of 1 L-MoS_2 might be just an overestimation caused by the capacitive coupling between the gates of the devices.[9] The work of Yoon *et al.* had also pointed out that 1 L-MoS_2 was not ideal for high-performance semiconductor device applications due to the heavy electron effective mass and the low electron mobility.[10] It is thus necessary to find 2D materials not only with sizable bandgap but also with large carrier mobility.

Recently, the 1 L-$PtSe_2$ (Fig. 1(a)) was synthesized by a straightforward and single-step method: the direct selenization at the Pt(111) substrate,[16] which was in contrast to conventional fabrication methods such as exfoliation[3,8] or chemical vapor deposition (CVD).[17,18] Although 1 L-$PtSe_2$ showed an indirect bangap of 1.2 eV, the photodegradation experiment based on 1 L-$PtSe_2$ found that the visible light induced degradation of methylene blue aqueous solution was about four times faster than that of the $PtSe_2$ nanocrystals, making 1 L-$PtSe_2$ in the same class as nitrogen-doped TiO_2 nanoparticles for photocatalysis.[16] Circular polarization calculations indicated the 1 L-$PtSe_2$ were a good candidate for valleytronics.[16] The group of Zhang found that the 1 L-$PtSe_2$ had the largest room temperature mobility (~3000 $cm^2/V/s$) among the studied 14 kinds of 1 L-TMDs.[19,20] The electron mobility of 1 L-$PtSe_2$ was even larger than the black phosphorus (1000 $cm^2/V/s$),[21,22] which was another kind of widely studied 2D material.[21–25] Very recently, the Raman spectroscopy measurement on $PtSe_2$ found the Raman active modes showed a clear intensity and position dependence with film thickness.[26] Yao *et al.* for the first time reported the experimental realization of unconventional R-2 Rashba effect in the 1 L-$PtSe_2$.[27] Li *et al.* found the indirect bandgap transformed to the direct one under uniaxial compressive strain.[28] In view of the simplicity of the production method, the ultra high electron mobility, the sizable bandgap, and good photocatalytic performance, the 1 L-$PtSe_2$ would be a promising 2D material in practical applications.

An emerging topic in 2D TMD research is the investigation of magnetism as most of the existing pristine 2D TMDs are intrinsically diamagnetic.[29–31] Previous experiment had

[a)]Author to whom correspondence should be addressed. Electronic mail: zhangw@nfpc.edu.cn

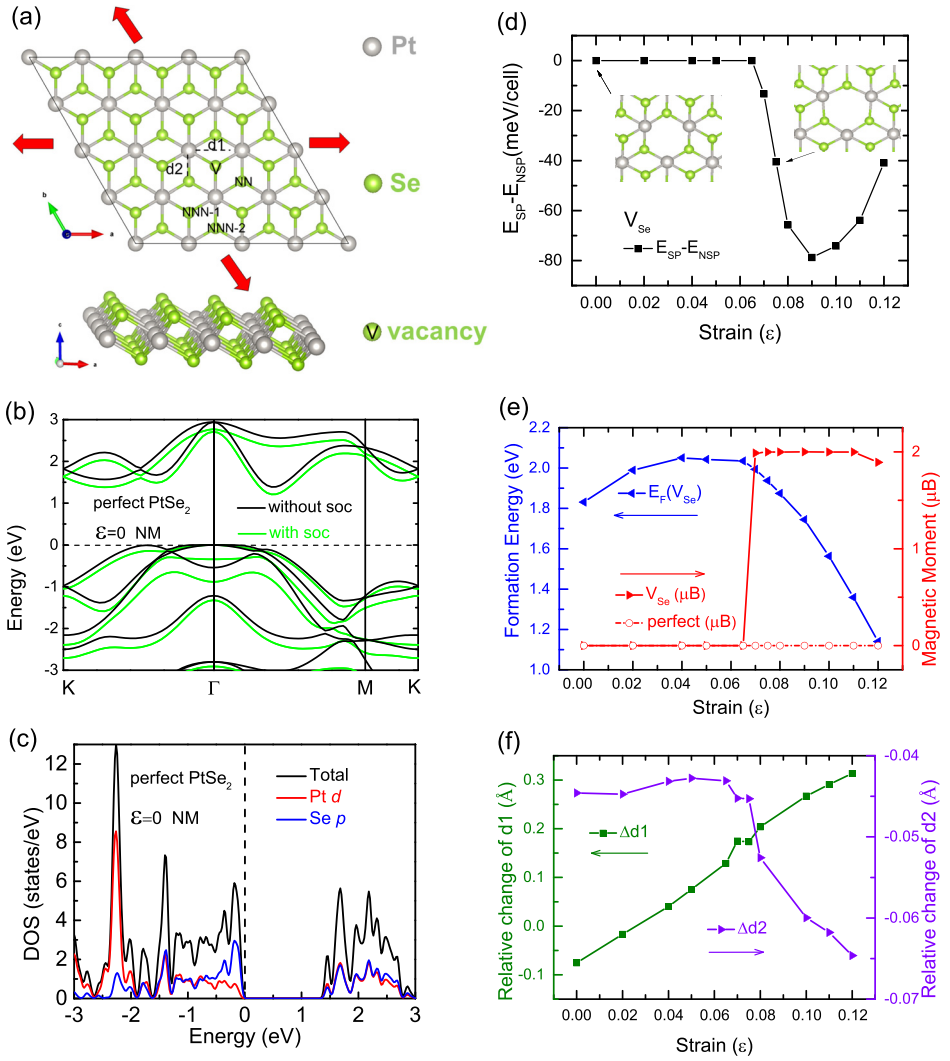

FIG. 1. (a) Topview (up panel) and sideview (down panel) of the $4 \times 4 \times 1$ supercell of 1 L-$PtSe_2$. NN and NNN denote the nearest neighboring Se atoms and the next nearest neighboring Se atoms around V_{Se}, respectively. d1 is the distance between the neighboring Pt atoms around V_{Se} while d2 is the distance between Pt atoms and NN Se atoms. (b) Bandstructures of perfect 1 L-$PtSe_2$. Note that the local VBM (between K and Γ) is about 9 meV smaller than the Γ point. The VBM is set as the Fermi level in this figure. (c) DOS of perfect 1 L-$PtSe_2$. (d) Total energies differences between the spin-polarized (SP) and spin-unpolarized (NSP) states. The insets show the crystal structures at selected strains. (e) Formation energy of V_{Se} and total magnetic moments. (f) Relative changes of d1 and d2.

shown that 1 L-TMDs could sustain strain up to about 11%.[32] The advantage of mechanical robustness made the strain to be a feasible approach to achieve a wide range controllability of the magnetic and electronic properties. The strain alone could not alter the magnetism of 1 L-MoS_2,[13–15] but the strain induced magnetism had been reported in 1 L-$NbSe_2$, 1 L-NbS_2,[33,34] and 1 L-TaX_2 (X = S, Se, and Te).[35,36] On the other hand, the 1 L-TMDs often had defects especially the chalcogen vacancy (V_X) during the process of exfoliation or CVD.[37] It had been experimentally reported that V_X can be easily formed by the electron beam.[38] Importantly, the crucial role played by vacancies in the magnetism of TMDs and graphene had been noticed in recent years. Furthermore, the magnetism was found on the strained 1 L-MoS_2 with V_S.[11] In this context, it is natural to think whether the strain and/or V_{Se} is able to provoke the magnetism in 1 L-$PtSe_2$. Current research interests of the 2D material also focus on the quest for nanoscale information storage devices with large magnetocrystalline anisotropy energy (MAE).[39–42] Typically, the reduced symmetry and the low dimensionality would induce appreciable MAE. The MA is a fundamentally relativistic effect and originates from the coupling between the orbital and spin degrees of freedom. Hence 5 *d* elements which possess strong spin orbit coupling (SOC) are potential candidates for magnetic nanostructures with large MAE. For instance, giant MAE had been found in the Pt-Ir dimer absorbed graphene.[41,42] Thus another question arises: Can 1 L-$PtSe_2$ or 1 L-$PtSe_2$ with V_{Se} has considerable MAE if they have magnetism?

The remainder of this paper is organized as follows: in Sec. II, we describe the calculation method used throughout this work. In Sec. III, we first study the magnetism of perfect 1 L-$PtSe_2$, and then present our results for the strain effect on the defective 1 L-$PtSe_2$ with V_{Se}. After that we discuss the origin of MAE. Finally, the conclusion is given in Sec. IV.

II. COMPUTATIONAL DETAILS

First-principles calculations are performed using the projector augmented wave (PAW) method,[43] as implemented in the vasp[44,45] code. The exchange-correlation functional is treated by the generalized gradient approximation (GGA).[46] The PAW potentials are used to describe the electron-ion interaction, with 10 valence electrons for Pt ($5d^9 6s^1$), 6 for Se ($4s^2 4p^4$). To model the vacancy, we construct a $4 \times 4 \times 1$ supercell with 48 atoms. A $5 \times 5 \times 1$ supercell is tested, and the main conclusions (e.g., the existence of magnetism) remain the same. Convergency tests show that the total

energy is more sensitive to the plane-wave cutoff energy than that of the k-point meshes. Thus, a plane-wave cutoff of 600 eV is used throughout. A $3 \times 3 \times 1$ and a $7 \times 7 \times 1$ k-point meshes[47] are used for the structural optimizations and density of states (DOS) calculations, respectively. Using these parameters, an energy convergence of less than 0.02 meV/atom is achieved. The crystal structures are relaxed until the inter-atomic forces are smaller than 0.01 eV/Å. A vacuum space of 15 Å in the direction normal to the layers is used to avoid the interactions between adjacent monolayers. In this work, we just consider the biaxial tensile strain. The case of uniaxial strain is also tested, but it is far less effective than the biaxial strain. The magnetism induced by uniaxial strain occurs at about 0.1 strain, and the magnetic moment is just 0.2 μB. The biaxial strain is defined $\epsilon = a/a_0 - 1$, where a_0 and a are the unstrained and strained lattice constants, respectively. The lattice constants are kept fixed at each strain while relaxing only internal coordinates of all atoms. The SOC is included in the calculations of MAE using the non-collinear mode of vasp, and the convergence criteria for total energy are 10^{-7} eV.

III. RESULTS AND DISCUSSION

A. Perfect 1 L-$PtSe_2$

The magnetism of perfect 1 L-$PtSe_2$ without strain is studied first. Except for the cases of ferromagnetic (FM) and nonmagnetic (NM), we also consider two types of antiferromagnetic orderings (AFM1[36] and AFM2[33,34,36]) which were recently proposed in the survey of the magnetism of perfect 1 L-TMDs. It is found that all the AFM states and the FM states relax to the NM states with equal total energies, indicating that the perfect 1 L-$PtSe_2$ without strain is NM, which agrees with the experiment.[16] As shown in Table I, the relaxed crystal structures agree well with the experiment[16] and the previous theoretical calculation.[49] Although the calculated theoretical bandgap without including SOC is a little larger than the experimental value, the experimentally observed indirect bandgap character is reproduced. As shown in Figs. 1(b) and 1(c), the valence band maximum (VBM) locates at the Γ point while the conduction band minimum (CBM) lies between Γ and M points. The Se *p* states in the VB play a major role around the Fermi level while the VB from −2 eV to lower energy are mainly made up by the Pt *d* states. The Pt *d* and Se *p* states contribute equally to the CB. As expected, the inclusion of SOC makes the degenerate bands at the VBM split into the non-degenerate ones and the CBM falls 0.2 eV; the predicted theoretical bandgap becomes the same as the experimental value. Then we explore the magnetism of 1 L-$PtSe_2$ under tensile strain. However, the 1 L-$PtSe_2$ is still NM whether or not the SOC is included, which reflect the expected fact that the six *d* electrons of Pt^{4+} (d^6) all stably occupy the t_{2g} orbitals and no magnetic orderings exist between Pt atoms. Thus, we can conclude that the 1 L-$PtSe_2$ is intrinsically nonmagnetic, and the biaxial strain alone cannot tune the magnetism of perfect 1 L-$PtSe_2$, which is similar to the case of 1 L-MoS_2.[13–15]

TABLE I. (a) The calculated lattice constants (a_0(b_0), Å), bond lengths ($b_{Pt\text{-}Se}$ and $b_{Se\text{-}Se}$, Å), bond angles ($\theta_{Se\text{-}Pt\text{-}Se}$, degree), and bandgap ($E_g$, eV) of perfect 1 L-$PtSe_2$. The value in parenthesis is calculated including the SOC. The experimental[16,48] (Exp.) data and theoretical[49] (The.) data are provided for comparison. (b) Formation energy (E_F, eV) of V_{Se} and V_{Pt}.

(a)	a_0	$b_{Pt\text{-}Se}$	$b_{Se\text{-}Se}$	$\theta_{Se\text{-}Pt\text{-}Se}$	E_g
Cal.	3.75	2.53	3.40	95.67	1.4(1.2)
The.[a]	3.75	2.53	3.40	95.63	1.41
Exp.[b]	3.73	2.51	3.35	96.13	1.2[c]

(b)	E_F (V_{Se})	E_F (V_{Pt})
Se poor	1.24	3
Se rich	1.83	4.19
Se rich[d]	1.81	
	1.82[e]	

[a]Reference 49.
[b]Reference 48.
[c]Reference 16.
[d]Calculated using $5 \times 5 \times 1$ supercell.
[e]References 38 and 52, calculated using $5 \times 5 \times 1$ supercell.

B. Stability of vacancies in 1L-$PtSe_2$

Next, we study the defective 1 L-$PtSe_2$ with vacancies. The vacancy formation energy is calculated according to the following formula:[51]

$$E_F(V) = E_{tot,v} - E_{tot,perfect} + \mu_v. \quad (1)$$

Here, μ_v is the chemical potential of Se or Pt. $E_{tot,\ perfect}$ and $E_{tot,\ v}$ denote the total energies of the perfect simulation cell and that containing one vacancy, respectively. The μ_v is related to the growth condition. In Se rich condition, μ_{Se} is subject to an upper bound given by the energy of Se in the bulk phase (hexagonal Se, $\mu_{Se} = \frac{1}{3}E_{Se_{hex}}$), which results in the lower limit on μ_{Pt} : $\mu_{Pt} = E_{tot,f.u.} - 2\mu_{Se}$. $E_{tot,f.u.}$ is the total energy of formula unit of perfect $PtSe_2$, i.e., $E_{tot,f.u.} = \frac{1}{16}E_{tot,perfect}$. In Se poor condition, μ_{Pt} is subject to an upper bound given by the energy of Pt in the bulk phase (fcc Pt, $\mu_{Pt} = \frac{1}{4}E_{Pt_{fcc}}$). Correspondingly, the upper limit on Pt results in a lower limit on Se: $\mu_{Se} = \frac{1}{2}(E_{tot,f.u.} - \mu_{Pt})$. As shown in Table I, the calculated E_F (V_{Se}) agrees with previous work[38,52] and is lower than E_F (V_S) of 1 L-MoS_2.[38] The E_F (V_{Pt}) is significantly larger than that of the E_F (V_{Se}), indicating that the V_{Se} is more prone to form than the V_{Pt}. This is not surprising since Pt atoms are covalently bonded to six neighboring Se atoms (see Fig. 2). The found stability of V_{Se} and V_{Pt} is consistent with previous report that the chalcogen vacancy can be easily formed in 1 L-TMDs while the formation of transition metal vacancy is highly unlikely due to the required higher electron energy which quickly destroys the chalcogen sublattice.[38] Therefore, in what follows, we focus on the discussion of V_{Se}.

C. Strain induced magnetism in 1 L-$PtSe_2$ with V_{Se}

In Subsection III A, we have shown that the strained perfect 1 L-$PtSe_2$ is NM. It is desirable to know whether there is magnetism in strained 1 L-$PtSe_2$ once the V_{Se} is introduced. As shown in Fig. 1(d), we calculate the total energy differences between spin-polarized (SP) and spin-unpolarized (NSP)

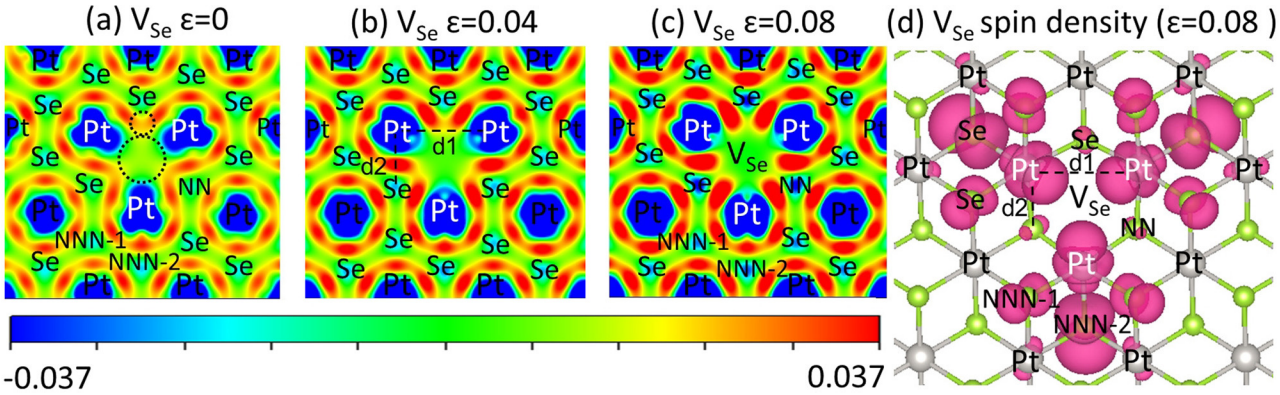

FIG. 2. (a)–(c) Differential charge density in the hexagonal plane of Pt atoms for V_{Se}. The reference charge density is the atomic charge density before bonding. The dashed circles denote the area among the three Pt atoms. The Pt atoms around (far away) the V_{Se} are marked by white (black). The units of the color scale are $e^-/Å^3$. Red and blue indicate the electron accumulation and depletion, respectively. (d)Spin density distribution of V_{Se} at $\epsilon = 0.08$. The violet isosurfaces correspond to positive spin density, and the isosurface value is $0.01\,e^-/Å^3$. Fig. 1(a) and Fig. 2 are plotted using VESTA.[50]

states. At first, the SP states relax to the NSP states with equal total energies, indicating the defective 1 L-$PtSe_2$ is NM when the strain is small. However, when the strain increases to 0.07, the SP states are favored as can be seen from the sudden decrease (increase) of total energy difference (magnetic moment). Fig. 1(e) shows that the total magnetic moments of the SP states are nearly kept fixed at 2 μB in the strain range, indicating the system is now FM. Encouragingly, the strain continually lowers the formation energy of V_{Se} when the system becomes FM. For example, the E_F (V_{Se}) at 0.09 strain is 1.74 eV, which is about 0.1 eV lower than the E_F (V_{Se}) at zero strain. Thus, when the system changes from NM to FM, the strain would help to increase the V_{Se} stability and promote to create the V_{Se}. However, Fig. 1(e) also shows that the E_F (V_{Se}) increases with respect to the strain when the strain is less than 0.04, which is unexpected. Generally speaking, the increase in bond lengths and volumes (for 3D materials) associated with the tensile strain is likely to decrease the formation energies of the vacancy[53–55] due to the dominant role of decreased Coulomb interactions between ions.[53] It is also believed that the remaining electrons of the vacancy would strengthen the pressure of the electron gas and thus induce an intrinsic compressive stress in the unrelaxed lattice. Therefore, the tensile strain would relieve the intrinsic compressive stress and help to create the vacancies.[56]

To understand the origin of the magnetism and the evolution of E_F (V_{Se}) with respect to the strain, we first examine the structural changes induced by the strain and V_{Se}. Fig. 1(f) shows the relative changes of concerned atoms, which is defined as the distance or bond length differences between defective and perfect 1 L-$PtSe_2$ at the corresponding strain. It can be seen that both Δd_1 and Δd_2 are negative at zero strain, which means that the Pt and/or Se atoms move closer to each other when the V_{Se} is created. Fig. 2(a) shows the charge density difference at zero strain. The electronic structures at zero strain are shown in Figs. 3(a) and 3(b). Fig. 2(a) shows clearly that there are large accumulations of electrons between Pt and Se atoms, and the distribution shapes of electrons exhibit directional character, which indicate that the Pt atoms are covalently bonded with the Se atoms. For the Pt atoms around the V_{Se}, there are obvious accumulations of electrons along the dashed line d1 (small circle area). There are also distributions of electrons (similar to "Y" shape) inside the hexagonal plane (big circle area). These results indicate that the Pt atoms around the V_{Se} are metallically bonded with each other. At the same time, the two Pt atoms are covalently bonded with the same nearest neighboring (NN) Se atom. Besides, there are some distributions of remaining electrons (Fig. 3(b)) of V_{Se} at the next nearest neighboring (NNN) Se atoms which are also covalently bonded with Pt atoms. Thus, the negative values of Δd_1 and Δd_2 at zero strain also reflect the stability of these bonds between concerned Pt and/or Se atoms. Because of the formation of these bonding states, the unsaturated spin electrons of V_{Se} are paired, thus the magnetism of Pt or Se atoms around V_{Se} is quenched, which is further confirmed by the symmetric DOS (not shown) for the SP states.

With the increase of strain, Δd_1 gradually increases. For Δd_2, it is negative on the whole strain range. When the strain increases to 0.04, Δd_1 becomes positive, indicating the Pt-Pt metallic bonds are weakened. This is consistent with the charge density difference in Fig. 2(b), where the charge accumulation between Pt atoms becomes less. Fig. 2(b) also shows the enhancement of the covalent bonds between Pt and Se_{NN} atoms, but Fig. 1(f) shows an irregular change of Δd_2 when the strain is less than 0.04, i.e., Δd_2 decreases first and then increases. Note that Δd_1 is an order of magnitude larger than Δd_2, thus the irregular change of Δd_2 indicates that the formation of metallic bonds play a dominant contribution to the structural changes of the system at small strain range, which restricts the change of Δd_2. When the strain increases to 0.07, both Δd_1 and Δd_2 show a discontinuity, which corresponds to the breaking of Pt-Pt metallic bonds shown in Fig. 2(c) where we can clearly see the vanish of accumulated electrons between Pt atoms. This leads to the formation of the nonbonding 5 *d* electrons of Pt atoms, and the magnetic moments are thus induced. Meanwhile the Pt-Se_{NN} covalent bonds are further enhanced as can be seen from the sharp decrease of Δd_2. Fig. 2(d) shows the spin density at 0.08 strain. The DOS at 0.08 strain are shown in Fig. 3(c). The corresponding band structures are shown in

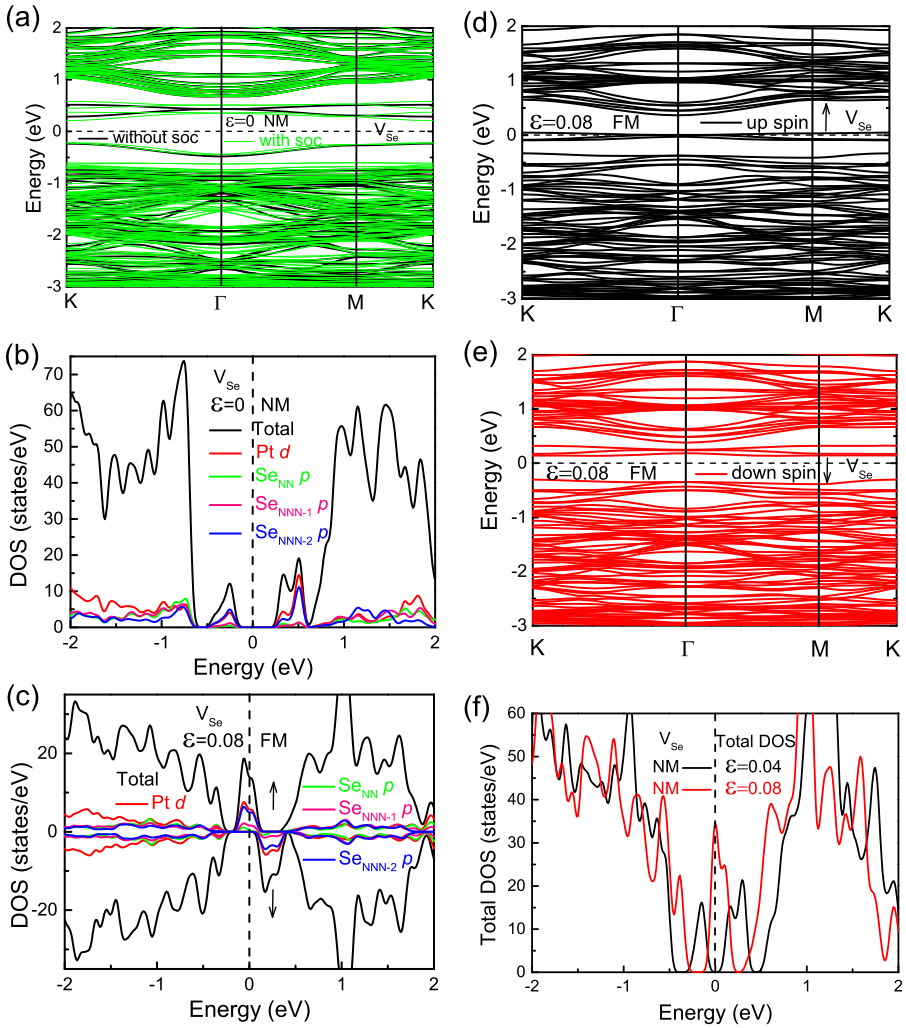

FIG. 3. (a) Band structure of 1 L-$PtSe_2$ with V_{Se} at zero strain. (b) DOS of 1 L-$PtSe_2$ with V_{Se} at zero strain. For convenience, all the Pt *d* and Se *p* states in this figure are magnified 6 times. (c) DOS of FM 1 L-$PtSe_2$ with V_{Se} at 0.08 strain. The up and down arrows denote the up-spin and down-spin states, respectively. The corresponding band structures are shown in (d) and (e). (f) Total DOS of NM 1 L-$PtSe_2$ with V_{Se} at different strain.

Figs. 3(d) and 3(e). We can see from Fig. 3(c) that there are two peaks in the gap, which correspond to the defect levels caused by V_{Se}. From Fig. 2(d), we can see the magnetic moments mainly arise from the states which constitute the defect levels (Fig. 3(c)). This can be ascribed to the spatially extended Pt 5*d* electrons (nonbonding) around the V_{Se}, which polarize the Pt atoms far away the V_{Se} and the NNN Se atoms. For the NN Se atoms, the Se_{NN} *p* states contribute very little to the defect levels, correspondingly very small magnetic moments ($\sim$0.01 μB) are found. The large spatial extensions of spin density are different from the case of defective 1 L-MoS_2 where the magnetic moments mainly distribute at the Mo sites around the V_S.[11] This difference can be attributed to the fact that the Pt 5*d* orbital is spatially more extensive than the Mo 4*d* one, which makes the defective 1 L-$PtSe_2$ easier to achieve the long range magnetic coupling at low defect concentrations.

Basing on above discussions, we propose a possible explanation to understand the behavior of E_F (V_{Se}) from the aspects of the competition between the bonds energies and the Coulomb interactions. As mentioned above, the creation of V_{Se} leads to the formation of metallic and covalent bonds. The stronger these bonds, the larger the energy are required to form these bonds. Although both the Pt-Pt metallic bonds and the Coulomb interactions become weak with the increase of strain, it is not able to compete with the enhanced Pt-Se covalent bonds at small strain range, thus the E_F (V_{Se}) increases at first. When the strain increases to 0.05, the further weakened Pt-Pt bonds and Coulomb interactions begin to play a dominant role of determining the E_F (V_{Se}), the E_F (V_{Se}) begins to decrease slightly. When the strain increases to the transition point of magnetism, i.e., $\epsilon = 0.07$, the metallic bonds are broken. The E_F (V_{Se}) now is determined mainly by the decreased Coulomb interactions. Thus, the E_F (V_{Se}) decreases quickly. Due to the lost of restrictions of Pt-Pt metallic bonds, the enhanced Pt-Se_{NN} bonds (Δd_2) become free to decrease rapidly to more negative values.

The magnetism can be further understood from the electronic structures. As shown in Figs. 3(a) and 3(b), the V_{Se} introduces two defect levels in the bandgap. The occupied bonding states are close to the VBM, and the unoccupied antibonding states lie near the CBM, which stabilizes the structure.[38] The defect levels are mainly occupied by Pt *d* and Se_{NNN} *p* states with a small contribution of Se_{NN} *p* states. The inclusion of SOC (Fig. 3(a)) makes a split in the defect bands, but the whole character (e.g., relative positions) of the defect states are kept and no magnetism is found. Within the Stoner theory of band ferromagnetism,[57] which is a mean field approach, the large DOS at the Fermi level ($N(E_F)$) is related to the instability of the NM state with

respect to the onset of intraband spin polarization, when $N(E_F)I > 1$. Here, I is the Stoner integral which was calculated and tabulated by Janak[58] for the elemental systems. As shown in Fig. 3(f), $N(E_F)$ is zero at 0.04 strain. However, a large $N(E_F)$ is obtained at 0.08 strain. As no I of Pt was reported by Janak, we approximately use the I of Rh (0.327 eV) and Pd (0.34 eV). The $N(E_F)$ of Pt is 10.53 eV^{-1}, and the estimated value of N_{Pt} $(E_F)I$ is about 3.44–3.58. Therefore, the large $N(E_F)$ clearly points to an unstable NM state. This is confirmed by the spin-polarized calculations shown in Fig. 3(c), where the imbalance between the occupied up-spin and down-spin states occurs. Therefore, the 1 L-$PtSe_2$ with V_{Se} shows a possible itinerant origin of magnetism or so-called Stoner ferromagnetism.[57] Fig. 3(c) shows that the Fermi level is mainly occupied by the Se p and Pt d states, and the similar picture (pd occupation) is obtained when SOC is included. Fig. 3(c) also shows that the system behaves as spin gapless semiconductors (SGS) which was proposed first by Wang[59] with fully spin-polarized electrons and holes. It had been experimentally reported that some SGS materials had been prepared which showed giant magnetoresistance, colossal electroresistance, and crossover of magnetoresistance.[60]

Before the ending this subsection, we study the magnetic coupling between the V_{Se} induced magnetic moments at 0.08 strain. This is because the existence of magnetic moments does not certainly result in magnetic coupling. We double the size of the previous supercell in the a direction, i.e., the supercell now contains two V_{Se} s with a distance of about 16.2 Å. Depending on the initial conditions of self-consistent calculations, two stable magnetic structures are obtained: one is AFM and the other is FM. The total energy difference ($\Delta E = E_{AFM} - E_{FM}$) between AFM and FM is $\Delta E = 23.7$ meV, indicating the FM coupling can be obtained even at such a long distance. This is understandable as the system displays the large spatial extensions of spin density at 0.08 strain (Fig. 2(d)). The polarized electrons between two V_{Se} s are able to effectively mediate an indirect long range FM coupling. Besides, to get more information about the strength of the FM coupling, we adopt a $5 \times 5 \times 1$ and a $6 \times 6 \times 1$ supercells to calculate the ΔE using the same procedure mentioned above. The $V_{Se} - V_{Se}$ distances in the expanded $5 \times 5 \times 1$ and $6 \times 6 \times 1$ supercells are about 20.3 Å and 24.3 Å, respectively. It is found that the ΔE decreases to 14.7 meV when the V_{Se}-V_{Se} distance is 20.3 Å, and the ΔE quickly decays to nearly zero (1 meV) when the V_{Se}-V_{Se} distance increases to 24.3 Å.

D. Magnetocrystalline anisotropy in 1 L-$PtSe_2$ with V_{Se}

Finally, let us discuss the found magnetocrystalline anisotropy. The magnetocrystalline anisotropy energy (MAE) is defined as $MAE = E_x\text{-}E_z$,[61] where E_x and E_z are the total energies of self-consistent calculations in the x and z magnetization directions, respectively. Therefore, the positive (negative) value of MAE represents the easy axis lies in the direction normal (parallel) to the $PtSe_2$ layer. As shown in Fig. 4(a), when the strain ranges from 0.075 to 0.09, the 1 L-$PtSe_2$ with V_{Se} has the easy magnetization direction normal to the layer and the maximum MAE is about 10.6 meV. When the strain ranges from 0.1 to 0.12, the easy axis lies in the in-plane direction with a maximum MAE of about 9 meV. The obtained maximum MAE is comparable with Ta(W) doped g-C_3N_4[41] and Pt-Fe dimer absorbed graphene with vacancy.[42] Above calculations indicate that the strain not only introduces magnetism for defective 1 L-$PtSe_2$, but also promotes the spin reorientation transition. The SOC Hamilton can be defined as $\hat{H}_{so} = \lambda \hat{L} \cdot \hat{S}$. $\hat{L}$ and $\hat{S}$ are the angular momentum and spin operator. λ is the strength of SOC. The MAE originates from the competition between

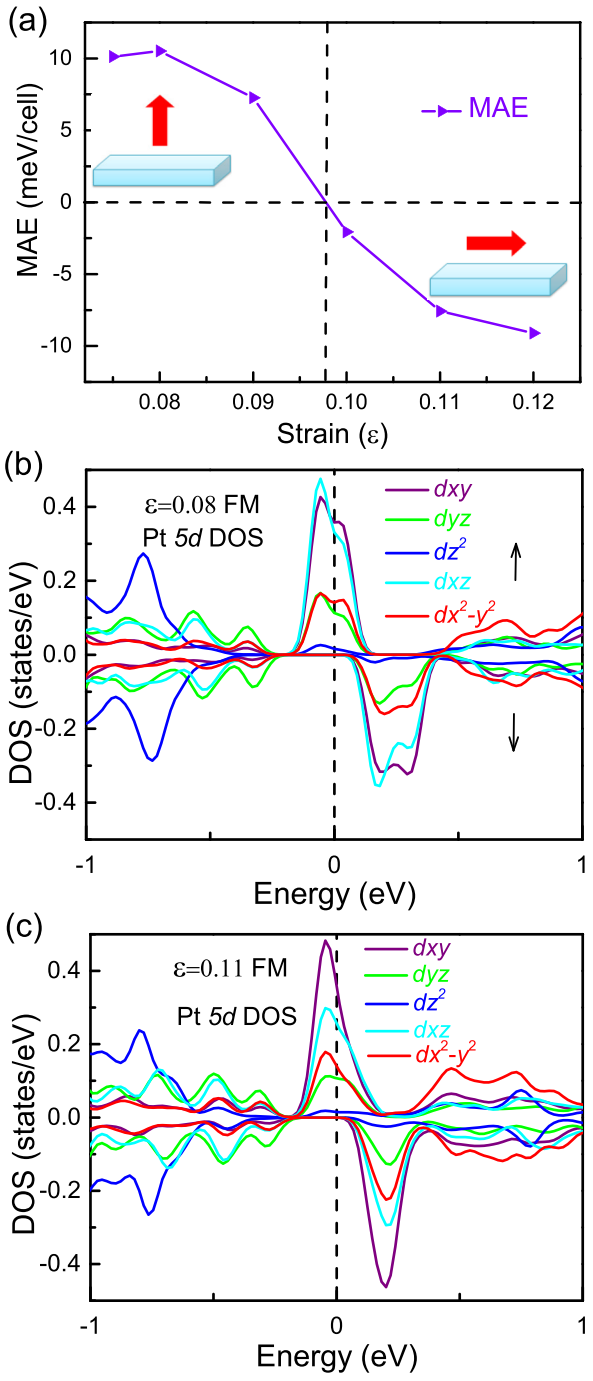

FIG. 4. (a) MAE with respect to the strain. (b) and (c) The Pt 5d DOS of FM 1 L-$PtSe_2$ with V_{Se} at 0.08 and 0.11 strain, respectively.

in-plane and perpendicular contributions of the SOC, which can be expressed as[61]

$$MAE = \lambda^2 \sum_{o,u,\alpha,\beta} (2\delta_{\alpha\beta} - 1) \times \left[\frac{|\langle o,\alpha|\hat{L}_z|u,\beta\rangle|^2}{E_{o,\alpha} - E_{u,\beta}} - \frac{|\langle o,\alpha|\hat{L}_x|u,\beta\rangle|^2}{E_{o,\alpha} - E_{u,\beta}} \right]. \quad (2)$$

Here, $E_{o,\alpha}$ and $E_{u,\beta}$ are the energy levels of the occupied states with spin $\alpha(\langle o,\alpha|)$ and unoccupied states with spin $\beta(|u,\beta\rangle)$. Clearly, heavy elements with large λ and narrow d bands are potential candidates for achieving giant MAE. The preferred magnetization orientation is determined by the nonzero matrix elements of $\hat{L}_x$ and $\hat{L}_z$ by different d states:[61] $\langle xz|\hat{L}_z|yz\rangle = 1$, $\langle x^2-y^2|\hat{L}_z|xy\rangle = 2$, $\langle xy|\hat{L}_x|xz\rangle = 1$, $\langle x^2-y^2|\hat{L}_x|yz\rangle = 1$, $\langle z^2|\hat{L}_x|xz,yz\rangle = \sqrt{3}$. When the spin directions of occupied and unoccupied states are the same, i.e., $\delta_{\alpha\beta}=1$, the positive(negative) contributions to MAE are the nonzero matrix elements of $\hat{L}_z(\hat{L}_x)$. For the occupied and unoccupied states with opposite spin directions, i.e., $\delta_{\alpha\beta}=0$, the positive(negative) contributions to MAE are the nonzero matrix elements of $\hat{L}_x(\hat{L}_z)$. We can qualitatively understand the driving forces for the MAE by analyzing the Pt 5*d* DOS. As shown in Fig. 4(b), there is a clear split for the states in the vicinity of the Fermi level. For the rest of the states, the DOS are nearly symmetric. The dz^2 states mainly locate at the positions far away the Fermi level while the states around the Fermi level are mainly occupied by the *dxy* and *dxz* orbitals. The main positive contribution to the MAE at 0.08 strain comes from the $\langle xz\uparrow|\hat{L}_z|yz\uparrow\rangle$, $\langle x^2-y^2\uparrow|\hat{L}_z|xy\uparrow\rangle$, $\langle xy\uparrow|\hat{L}_x|xz\downarrow\rangle$, and $\langle x^2-y^2\uparrow|\hat{L}_x|yz\downarrow\rangle$. Although the $\langle xy\uparrow|\hat{L}_x|xz\uparrow\rangle$ would provide large negative contribution to the MAE, the $|\langle x^2-y^2\uparrow|\hat{L}_z|xy\uparrow\rangle|^2$ is four times of $|\langle xy\uparrow|\hat{L}_x|xz\uparrow\rangle|^2$. The $\langle x^2-y^2\uparrow|\hat{L}_z|xy\downarrow\rangle$ also contribute negatively to the MAE, and the corresponding $E_{o,\alpha}$–$E_{u,\beta}$ is larger than that of the $\langle x^2-y^2\uparrow|\hat{L}_z|xy\uparrow\rangle$. Besides, the negative contribution provided by $\langle x^2-y^2\uparrow|\hat{L}_z|xy\downarrow\rangle$, $\langle xy\uparrow|\hat{L}_x|xz\uparrow\rangle$ and other nonzero matrix elements can also be canceled by the positive contributions mentioned above. Therefore, there are still net positive contributions to the MAE at 0.08 strain. Comparing with the relative distribution of different *d* states at 0.08 strain, the DOS at 0.11 strain (Fig. 4(c)) does not show too much obvious change for the occupied *d* states in the energy range of ∼−0.2–−1 eV. The main changes are the relative increase (decrease) of *dxy*(*dxz*) states in the vicinity of the Fermi level. Besides, there is more distribution of unoccupied dx^2-y^2 states at 0.11 strain. Therefore, the spin reorientation transition is mainly caused by the increase of *dxy*(dx^2-y^2) states and the decrease of *dxz* states.

IV. CONCLUSION

In summary, we have studied the magnetic and electronic properties of the newly synthesized 1 L-TMD $PtSe_2$ using first-principles calculations. Consistent with previous work, we find V_{Se} is more prone to form than V_{Pt}. It is found that the strain or V_{Se} alone cannot lead to the magnetism. However, the magnetism can be introduced by an interplay between strain and V_{Se}. The induced magnetism originates from the breaking of the Pt-Pt metallic bonds. Different from the case of 1 L-MoS_2 with V_S, the defective 1 L-$PtSe_2$ has the spatially extended spin density, because of which the long range ferromagnetic coupling is obtained. Besides, we find the 1 L-$PtSe_2$ with V_{Se} undergoes a spin reorientation transition from out-of-plane to in-plane magnetization and the obtained maximum MAE is ∼9–10.6 meV/V_{Se}. Our calculations indicate that the strain not only can effectively tune the magnetism but also can manipulate the magnetization direction of 1 L-TMDs.

ACKNOWLEDGMENTS

Wei Zhang would like to thank Dr. Weixiao Ji, Xiaohui Wang, Deyu Li (SSC), and Qingwei Hao (SDSC) for their help in our research. This work was supported by the basic research project of central university (Grant Nos. LGYB201610, LGYB201612, and LGYB201609,). First-principles calculations are performed at the Shanghai Supercomputer Center. Part of the supercomputer time is provided by the HPC Center of Department of Physics at the Nanjing Normal University.

[1]K. S. Novoselov, A. K. Geim, S. V. Morozov, D. Jiang, Y. Zhang, S. V. Dubonos, I. V. Grigorieva, and A. A. Firsov, Science **306**, 666 (2004).
[2]K. S. Novoselov, A. K. Geim, S. V. Morozov, D. Jiang, M. I. Katsnelson, I. V. Grigorieva, S. V. Dubonos, and A. A. Firsov, Nature (London) **438**, 197 (2005).
[3]K. S. Novoselov, D. Jiang, T. J. Booth, W. Khotkevich, S. V. Morozov, and A. K. Geim, Proc. Natl. Acad. Sci. U.S.A. **102**, 10451 (2005).
[4]Q. H. Wang, K. Kalantar-Zadeh, A. Kis, J. N. Coleman, and M. S. Strano, Nat. Nanotechnol. **7**, 699 (2012).
[5]T. Heine, Acc. Chem. Res. **48**, 65 (2015).
[6]F. Schwierz, Nat. Nanotechnol. **5**, 487 (2010).
[7]Y. Wu, Y. M. Lin, A. A. Bol, A. Jenkins, F. Xia, D. B. Farmer, Y. Zhu, and P. Avouris, Nature (London) **472**, 74 (2011).
[8]B. Radisavljevic, A. Radenovic, J. Brivio, V. Giacometti, and A. Kis, Nat. Nanotechnol. **6**, 147 (2011).
[9]M. S. Fuhrer and J. Hone, Nat. Nanotechnol. **8**, 146 (2013).
[10]Y. Yoon, K. Ganapathi, and S. Salahuddin, Nano Lett. **11**, 3768 (2011).
[11]H. L. Zheng, B. S. Yang, D. D. Wang, R. L. Han, X. B. Du, and Y. Yan, Appl. Phys. Lett. **104**, 132403 (2014).
[12]P. Tao, H. H. Guo, T. Yang, and Z. D. Zhang, J. Appl. Phys. **115**, 054305 (2014).
[13]E. Scalise, M. Houssa, G. Pourtois, V. Afanasev, and A. Stesmans, Nano Res. **5**, 43 (2012).
[14]P. Johari and V. B. Shenoy, ACS Nano **6**, 5449 (2012).
[15]T. S. Li, Phys. Rev. B **85**, 235407 (2012).
[16]Y. L. Wang *et al.*, Nano Lett. **15**, 4013 (2015).
[17]A. M. VanderZande *et al.*, Nat. Mater. **12**, 554 (2013).
[18]A. L. Elías *et al.*, ACS Nano **7**, 5235 (2013).
[19]W. X. Zhang, Z. S. Huang, W. L. Zhang, and Y. R. Li, Nano Res. **7**, 1731 (2014).
[20]Z. S. Huang, W. X. Zhang, W. L. Zhang, and Y. R. Li, e-print arXiv:1505.05698.
[21]L. Li, Y. Yu, G. J. Ye, Q. Ge, X. Ou, H. Wu, D. Feng, X. H. Chen, and Y. Zhang, Nat. Nanotechnol. **9**, 372 (2014).
[22]H. Liu, A. T. Neal, Z. Zhu, Z. Luo, X. Xu, D. Tománek, and P. D. Ye, ACS Nano **8**, 4033 (2014).
[23]E. S. Reich, Nature (London) **506**, 19 (2014).
[24]J. Dai and X. C. Zeng, J. Phys. Chem. Lett. **5**, 1289 (2014).
[25]M. Buscema, D. J. Groenendijk, G. A. Steele, H. S. J. VanderZant, and A. Castellanos-Gomez, Nat. Commun. **5**, 4651 (2014).
[26]M. O'Brien *et al.*, 2D Materials **3**(2), 021004 (2016).
[27]W. Yao *et al.*, e-print arXiv:1603.02140.
[28]P. F. Li, L. Li, and X. C. Zeng, J. Mater. Chem. C **4**, 3106–3112 (2016).
[29]A. Kuc, N. Zibouche, and T. Heine, Phys. Rev. B **83**, 245213 (2011).

[30]Z. Y. Zhu, Y. C. Cheng, and U. Schwingenschlogl, Phys. Rev. B **84**, 153402 (2011).
[31]C. Ataca, H. Sahin, and S. Ciraci, J. Phys. Chem. C **116**, 8983 (2012).
[32]S. Bertolazzi, J. Brivio, and A. Kis, ACS Nano **5**, 9703 (2011).
[33]Y. G. Zhou, Z. G. Wang, P. Yang, X. T. Zu, L. Yang, X. Sun, and F. Gao, ACS Nano **6**, 9727 (2012).
[34]Y. Xu, X. F. Liu, and W. L. Guo, Nanoscale **6**, 12929 (2014).
[35]H. Y. Guo, N. Lu, L. Wang, X. J. Wu, and X. C. Zeng, J. Phys. Chem. C **118**, 7242 (2014).
[36]P. Manchanda, V. Sharma, H. B. Yu, D. J. Sellmyer, and R. Skomski, Appl. Phys. Lett. **107**, 032402 (2015).
[37]W. Zhou, X. L. Zou, S. Najmaei, Z. Liu, Y. M. Shi, J. Kong, J. Lou, P. M. Ajayan, B. I. Yakobson, and J. C. Idrobo, Nano Lett. **13**, 2615 (2013).
[38]H. Komsa, J. Kotakoski, S. Kurasch, O. Lehtinen, U. Kaiser, and A. V. Krasheninnikov, Phys. Rev. Lett. **109**, 035503 (2012).
[39]R. Wiesendanger, Rev. Mod. Phys. **81**, 1495 (2009).
[40]D. Sellmyer and R. Skomski, *Advanced Magnetic Nanostructures* (Springer, New York, 2006).
[41]Y. Zhang, Z. Wang, and J. X. Cao, J. Mater. Chem. C **2**, 8817 (2014).
[42]J. Hu and R. Q. Wu, Nano Lett. **14**, 1853 (2014).
[43]P. E. Blöchl, Phys. Rev. B **50**, 17953 (1994).
[44]G. Kresse and J. Furthmüller, Phys. Rev. B **54**, 11169 (1996).
[45]G. Kresse and D. Joubert, Phys. Rev. B **59**, 1758 (1999).
[46]J. P. Perdew, K. Burke, and M. Ernzerhof, Phys. Rev. Lett. **78**, 1396 (1997).
[47]H. J. Monkhorst and J. D. Pack, Phys. Rev. B **13**, 5188 (1976).
[48]S. Furuseth, K. Selte, and A. Kjekshus, Acta. Chem. Scand. **19**, 257 (1965).
[49]H. L. Zhuang and R. G. Hennig, J. Phys. Chem. C **117**, 20440 (2013).
[50]K. Momma and F. Izumi, J. Appl. Crystallogr. **41**, 653 (2008).
[51]C. Freysoldt, B. Grabowski, T. Hickel, J. Neugebauer, G. Kresse, A. Janotti, and C. G. VandeWalle, Rev. Mod. Phys. **86**, 253 (2014).
[52]Note that in Ref. 38 Komsa *et al*. did not consider the spin-polarization to calculate the total energy of isolated chalcogen atoms for their purpose of research (private communication). In order to avoid misunderstanding and to compare directly, we use the energy of spin-polarized Se atom and provide the converted $E_F(V_{Se})$ basing on the original data of Komsa *et al*.
[53]U. Aschauer, R. Pfenninger, S. M. Selbach, T. Grande, and N. A. Spaldin, Phys. Rev. B **88**, 054111 (2013).
[54]Q. Yang, J. X. Cao, Y. Ma, Y. C. Zhou, L. M. Jiang, and X. L. Zhong, J. Appl. Phys. **113**, 184110 (2013).
[55]D. W. Ma, Z. S. Lu, Y. N. Tang, T. X. Li, Z. J. Tang, and Z. X. Yang, Phys. Lett. A **378**, 2570 (2014).
[56]J. Zhu, F. Liu, G. B. Stringfellow, and S. H. Wei, Phys. Rev. Lett. **105**, 195503 (2010).
[57]P. Mohn, *Magnetism in the Solid State* (Springer-Verlag, Berlin, 2003).
[58]J. F. Janak, Phys. Rev. B **16**, 255 (1977).
[59]X. L. Wang, Phys. Rev. Lett. **100**, 156404 (2008).
[60]S. Ouardi, G. H. Fecher, and C. Felser, Phys. Rev. Lett. **110**, 100401 (2013).
[61]D. S. Wang, R. Q. Wu, and A. J. Freeman, Phys. Rev. B **47**, 14932 (1993).